Proceedings of the 2007 International LWR Fuel Performance Meeting
San Francisco, California, September 30 – October 3, 2007
Paper 1032

# Fracture of Hydrided Zircaloy-4 Sheet under Through-Thickness Crack Growth Conditions

P. A. Raynaud [1], D. A. Koss [1], A. T. Motta [2], and K. S. Chan [3]
[1] *Department of Materials Science and Engineering, The Pennsylvania State University, University Park, PA 16802*
[2] *Department of Mechanical and Nuclear Engineering, The Pennsylvania State University, University Park, PA 16802*
[3] *Southwest Research Institute, San Antonio, TX 78238*

**Abstract –** *The failure of thin-wall components such as fuel cladding may be caused by crack initiation on the component surface and subsequent crack growth through its thickness. This study has determined the fracture toughness of hydrided cold-worked stress relieved Zircaloy-4 sheet subject to through-thickness crack growth at 25°C. The experimental approach utilizes a novel procedure in which a narrow linear strip of brittle hydride blister across the specimen width creates a well-defined pre-crack upon initial loading. The subsequent crack growth resistance is then characterized by four-point bending of the specimen and an elastic-plastic fracture mechanics analysis. At room temperature, the through-thickness fracture toughness ($K_Q$) is sensitive to the orientation of the hydride platelets, and $K_Q \cong 25$ MPa$\sqrt{m}$ for crack growth through a mixed in-plane/out-of-plane hydride field. In contrast, $K_Q$ is much higher ($\cong 75$ MPa$\sqrt{m}$) when the hydride platelets are oriented predominantly in the plane of the sheet (and therefore normal to both the crack plane and the crack growth direction). The implication of these fracture toughness values to the fracture strain behavior of hydrided Zircaloy-4 under through-thickness crack growth conditions is illustrated.*
*Keywords: Zircaloy, hydrides, fracture toughness*

## I. INTRODUCTION

The ductility of thin-wall zirconium components such as nuclear fuel cladding can be degraded by hydrogen ingress associated with waterside corrosion during reactor exposure. The resulting uptake of hydrogen has long been identified as a main contributor to limiting the fracture resistance of cladding at high burnup levels [1, 2]. For thin-wall components such as cladding, the most severe form for hydrogen-induced loss of ductility occurs when a surface crack initiates within a hydride rim or blister and subsequently propagates in a *through-thickness crack-growth mode* [3-6]. In order to predict the cladding performance/ductility under such a "worst-case" condition under quasi-static loading , it is essential to know the following: (a) the initial crack depth resulting from fracture initiation at a hydride rim or blister, (b) the relevant hydride microstructure (i.e., radial v. circumferential hydrides) through which the crack subsequently grows to failure, (c) the appropriate temperature (or range of temperatures), (d) the stress state under which deformation and fracture occurs, and importantly (e) the fracture toughness under through-thickness crack growth conditions for the appropriate temperature and hydride microstructure.

While the fracture toughness behavior of hydrided zirconium alloys components has been determined for crack growth across the width of plate material, the fracture toughness for through-thickness crack growth of a thin-wall Zircaloy cladding in the hydrided condition is yet to be determined. The closest relevant study is that in which the toughness has been determined for hydrided Zircaloy cladding tubes for crack growth along the tube axis [7]. In that case, the plane stress condition at the crack tip dictates mixed mode I/III crack propagation; in contrast, crack growth through the thickness of a cladding tube will very likely occur under a plane-strain condition along the crack front, and it should be accompanied by an elevated degree of plastic constraint through the wall thickness; either mode I or mixed mode I/II crack growth are likely. Thus, the crack-tip plasticity and damage accumulation process that dictate through-thickness crack growth in a thin-wall component will likely give rise to fracture toughness values at variance with those obtained in conventional fracture toughness tests.

In addition to the damage mechanics considerations, researchers [8-10] have recognized that fracture toughness is sensitive to the morphology and orientation of the hydride platelets with respect to both the crack plane and crack growth direction. In the present case, the fracture toughness under a through-thickness crack growth condition in textured *and* hydrided zirconium alloy also creates a crack plane/crack growth direction condition which differs from those of previous fracture toughness studies. For example, hydride platelets aligned in the plane of sheet material (akin to circumferential hydrides in cladding tubes) will be oriented normal to both the crack plane *and* the crack growth direction during through-thickness crack growth. In contrast, out-of-plane hydrides (such as radial hydrides in cladding tubes) would align with both the crack plane and crack growth direction during through-thickness crack growth. Much different fracture toughness values would be expected between these two hydride morphologies.

Utilizing a novel experimental procedure, this study has determined the room temperature fracture toughness of unirradiated but hydrided cold-worked and stress-relieved (CWSR) Zircaloy-4 sheet subject to *through-thickness* crack growth as influenced by hydride microstructure. As an illustration of the implications of the fracture toughness values, the failure strain behavior of thin-wall hydrided Zircaloy-4 is predicted as a function of crack depth and compared to previous experimental observations of Zircaloy containing either a hydride blister or a dense rim of hydride particles. As a result, this study should be relevant to the development of codes designed to predict the mechanical performance of hydrided thin-wall reactor components under crack-limiting conditions.

## II. EXPERIMENTAL PROCEDURE

The material used in this study is Zircaloy-4 sheet, 675μm thick, obtained from Teledyne Wah-Chang initially in the cold-worked (CW) state. The specimens were subsequently annealed in a vacuum furnace at $10^{-6}$ Torr and 520°C for two hours in order to obtain a cold-worked-stress-relieved (CWSR) material state. The Kearns texture parameters [11] were determined to be similar to those previously reported for Zircaloy-4 cladding tube [12, 13] if the three orthogonal directions of the sheet were appropriately aligned with those of the cladding tube. Thus, the Kearns parameters were 0.57 in normal to the sheet surface, 0.34 transverse to the rolling direction, and 0.16 in the rolling direction. These values compare favorably with the corresponding values of 0.58, 0.32, and 0.10 in the radial, circumferential, and axial orientations (respectively) of Zircaloy-4 cladding tubes [5].

Tensile testing of the CWSR Zircaloy-4 sheet resulted in a yield strength (597 MPa) and plastic anisotropy parameter of R = (width strain/thickness strain) = 2.6 in the transverse orientation of the sheet. Both of these values are similar to those of CWSR Zircaloy-4 cladding tube at 25°C, where the yield stress is ≈ 610 MPa and R ≅ 2.3 in the hoop orientation of the tube [6]. However, the strain-hardening exponent ($n = d\ln\sigma/d\ln\varepsilon$, where σ and ε are true stress and true strain, respectively.) was significantly smaller of this sheet material (n = 0.009) in the transverse orientation than n = 0.059 for cladding tube transverse to the tube axis [5]. In fact, the strain hardening behavior of this sheet material is similar to that of irradiated cladding [13].

To determine the fracture toughness, a novel experimental procedure was developed in which a narrow 200-700μm wide linear strip of hydride blister is created across the width of Zircaloy-4 sheet specimen for the purpose of generating a well-defined pre-crack upon loading. In order to form a "linear" hydride blister of controlled depth, the Zircaloy-4 specimen was first immersed in a solution of nitric acid (10 parts), $H_2O$ (10 parts) and hydrofluoric acid (1 part) for ~30s to remove the native oxide layer. Then a gold layer was sputter-deposited on both surfaces of the specimen to act as a barrier to hydrogen diffusion into the substrate. A diamond scribe was then used to remove a thin strip of gold (~ 100μm wide) across the specimen width. Immediately after removal of the thin gold strip, the specimen was coated with a ≈ 20 nm thick layer of nickel (99.995% pure) to create a "window" for hydrogen pickup along the thin strip where the gold was removed.

The specimens were then hydrogen-charged at 370°C under a finite volume of mixture of argon and hydrogen gas (12.5% $H_2$, balance argon) for times ranging from 20 minutes to 120 minutes. Subsequent annealing was performed for 10 minutes at 400°C and followed by furnace cooling. Cross-sectional metallographic examinations showed that the blister depth within a given specimen (~50 to ~320 μm) was relatively uniform across the width of the sample, as determined from both cross section metallography and the fracture surface after the test. As will be described later, the microstructure beneath the solid blister consisted of discrete hydride precipitate particles with a range of morphologies that depended on the depth of the blister.

Fracture toughness testing was performed using the four-point bend fixture shown in Fig. 1. This specimen configuration allowed uniform bending between the center loading pins, which were sufficiently far apart that the stress fields resulting from the pin contact did not affect crack growth under the hydride blister. The top of the bend fixture had a V-shaped groove normal to the axial direction of the loading pins, and a 2 mm pin was placed in this groove in order to suppress any bending moment transfer to the crack induced by the contact between the upper ram and the top of the fixture.

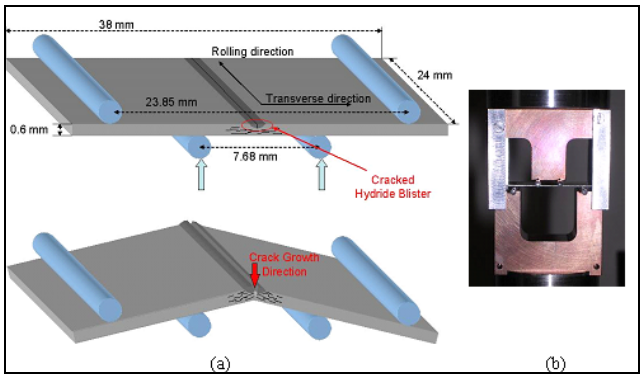


Fig. 1. (a) A schematic drawing of the four point bend specimen and (b) photo of the test fixture with a specimen loaded.

For the purpose of determining the initial crack length as accurately as possible, the four-point bend specimens (initially ≈32 mm, 38 mm in length, and ≈0.6 mm in thickness) were pre-cracked by a small amount of bending, and using acoustic emission signals emitted from the specimen to detect the cracking events. At loads less than necessary to cause substrate yielding, blister cracking was easily identified and the crack depth was determined from two ≈ 4 mm slices taken from each edge of the specimen. In some cases, more than one deep crack would form within the blister, invalidating the test. Bend testing of the pre-cracked specimen was performed in a screw-driven Instron machine with a crosshead displacement rate of 0.5 mm/minute. For some of the tests, the crack growth behavior was determined in a continuous manner using the electric potential drop (EPD) technique [14] using both notched and pre-cracked specimens to benchmark the crack length/potential drop response.

Given the level of plastic deformation that accompanies crack growth in the current study, elastic-plastic fracture mechanics were used to predict crack growth behavior. We relied on the ASTM E1820 procedure to determine the critical J-integral value at the onset of crack growth initiation during the load-displacement response:

$$J_{tot} = J_{el} + J_{pl} = \frac{K_i^2 \cdot \left(1-\nu^2\right)}{E} + J_{pl} \qquad (1)$$

$$J_{pl} = \frac{\eta \cdot A_{pl}}{B_N \cdot b_o} \qquad (2)$$

where $J_{el}$ and $J_{pl}$ are the elastic and plastic components of J-integral, respectively; $K_i$ is the stress intensity factor; ν is Poisson's ratio; E is Young's modulus; $a_i$ is the crack length; $B_N$ and W are the width and thickness of the specimen, respectively; $b_o$ =W-$a_o$ is the initial length of the remaining ligament; $A_{pl}$ is the amount of plastic energy spent by the applied load (the plastic energy under the load-displacement curve); and η is a geometric factor which depends on crack length.

In Eq. 1, the magnitude of the elastic stress intensity factor $K_i$ can be readily determined for our specimen geometry [15]. As seen in Eq. 2, the magnitude of $J_{pl}$ is directly dependent on the magnitude of the η parameter, and for small cracks, the η parameter is quite sensitive to the ($a_i$/W)-value. This condition is not an issue in conventional fracture toughness testing where $a_i$/W = 0.5 (for which η = 2 and is insensitive to small changes of crack length). However, for cladding tube performance where small surface cracks may occur, it is of interest to establish the fracture toughness at small crack lengths, $a_i$/W < 0.5, which is a range where the value of η changes rapidly with crack length. Several recent studies [16-18] have used finite element modeling to calculate η for conventional four-point bend geometries which respect the ASTM requirements. For example, Kim's results, which were obtained for thick plate configurations, show η depends on crack length as follows:

$$\eta = \begin{cases} 0.38 + 8.1(a/W) - 9.0(a/W)^2 & for\ a/W < 0.3 \\ 2 & for\ a/W \geq 0.3 \end{cases} \qquad (3)$$

Recalling Eq. 1 and assuming a plane-strain condition along the crack front, we can then obtain the $K_Q$ -value for the crack growth initiation toughness from

$$K_Q = \sqrt{\frac{J_{tot} E}{\left(1-\nu^2\right)}} \qquad (4)$$

In the present study, the specimen geometry/test procedure and crack growth resistance often resulted in a detectable load drop associated with the onset of crack growth initiation. Thus, $K_Q$ was defined on the basis of the first detectable onset of crack growth or load drop, rather than on the basis of conventional offset load-line displacement procedure as specified in ASTM 1820 for elastic-plastic crack growth analysis. Furthermore, it is readily recognized that the small thicknesses (≈ 0.6 mm) of these sheet specimens also do not meet ASTM specifications.

## III. RESULTS AND DISCUSSION

### *III.A. Hydride Microstructure*

The experimental hydrogen-charging procedure, which is the basis for inducing a pre-crack within the strip of solid hydride blister extending across the specimen width, also creates a microstructure consisting of hydride particles beneath the hydride blister. As summarized in Table 1, depending on blister depth, two distinct hydride microstructures were formed in the region of crack growth initiation near the hydride blisters, and as a result, two different fracture toughness values result.

For the case of small blisters (i.e., less than about 120 μm deep) as shown in Fig. 2a, the hydride microstructure in the region directly below the hydride blister, (where crack growth initiation occurs), consists of elongated hydride particles oriented within the plane of the sheet. These "in-plane" hydrides correspond to the "circumferential" hydrides in cladding tubes. Among the in-plane hydrides, there exists a small population of large hydrides with lengths in excess of 100 μm; as will be shown later, these large hydrides serve as the primary void sites for crack growth. Importantly, all of the in-plane hydrides are *oriented* normal to the crack plane. Thus, akin to through-thickness crack growth in Zircaloy cladding tubing containing "circumferential" hydrides, the propagating crack intersects the broad faces of the hydride platelets, and as will be shown, the resulting fracture toughness is comparatively high.

In contrast, test specimens with large hydride blisters, such as depicted in Fig 2b, exhibit three distinct forms of hydrides present within the Zircaloy substrate beneath the blister. As summarized in Table 1, in addition to the solid hydride blister (whose depth is roughly one-half of its width), the microstructures beneath blisters that are more than about 140 μm deep contain three zones the size of which increase with blister depth:

1. "Sunburst hydrides" Emanating radially from and connected to the hydride blister are "sunburst hydrides" which extend a finite distance beneath the blister. In the Figure 2b, the zone of sunburst hydrides is on the order of 100 μm.
2. "Mixed hydride zone": Adjacent to the sunburst hydrides, there is a transition zone within which discrete hydride particles with mixed orientations are present. A significant fraction of these mixed hydrides have their platelet surfaces oriented parallel to the crack plane *and* in the crack growth direction (i.e. these are akin to radial hydrides within a cladding tube). For large blisters, the depth of the mixed hydride zone increases with increasing blister depth. The size of the "mixed hydride zone" on Figure 2b is also on the order of 100 μm.
3. "In-Plane Hydride Zone": Finally, the remainder of the Zircaloy sheet contains discrete hydride platelets that are parallel to the sample surface and thus perpendicular to the crack growth direction *and* the crack plane (in-plane hydrides), as seen throughout the thickness in samples containing thinner blisters (see Figure 2a). These hydrides are akin to the "circumferential hydrides", typically observed in Zircaloy cladding tubes.

While the hydride microstructures were relatively uniform across the *width* of the blister, the small volume of sheet material that was charged with hydrogen made it impossible to use chemical means to determine the actual hydrogen contents of the Zircaloy directly beneath the blister through which crack propagation occurs. However, the average inter-particle spacing of the *in-plane* hydrides was determined for each individual test specimen, and these values were roughly independent of both blister depth and specimen location, suggesting that specimens with different blister depths had similar and relatively uniform hydrogen contents within the substrate beneath the hydride blister.

TABLE I

A summary of the hydride microstructures beneath the hydride blister within test specimens with differing ranges of blister depth.

| **Hydride Blister Depth** | **Substrate Hydride Microstructures Beneath Blister** |
|---|---|
| Small blisters, less than ≈ 120 μm deep | 1. Elongated "in-plane" hydrides oriented in plane of the sheet ($K_Q$ is thus for crack growth into an in-plane hydride microstructure). |
| Large blisters, greater than ≈ 140 μm deep | 1. Sunburst hydrides emanating from blister.<br>2. Mixed hydrides region between the sunburst and in-plane hydrides. (For these specimens, $K_Q$ relates to crack growth into a mixed hydride microstructure)<br>3. In-plane hydrides in remainder of specimen thickness |

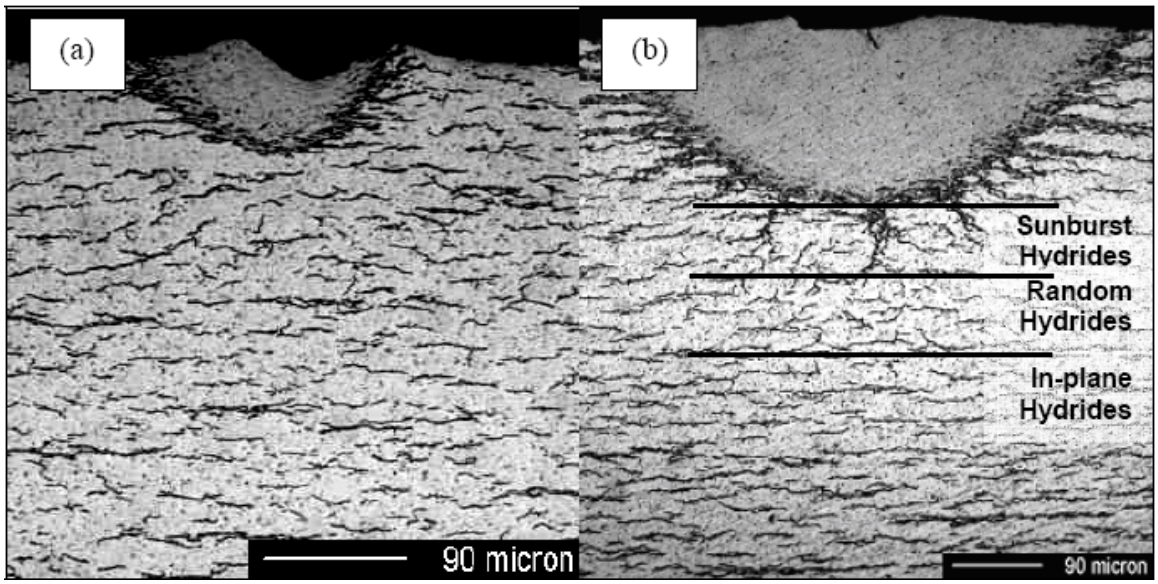


Fig. 2. Light micrographs of the cross section of a specimen with a blister depth of (a) ~ 60 μm and (b) ~ 210 μm. Note presence of sunburst and random hydride zone beneath the deeper blister in (b).

*III.B. Fracture Toughness and Hydride Microstructure*

Solid hydride blisters are known to be brittle at temperatures up to at least 400º C [19], and examinations of bend specimens after initial loading showed that the hydride blister cracked prior to any large scale plastic deformation of the substrate. Once the blister cracks, the subsequent crack growth behavior depends on the character of the substrate hydride microstructure.

In the case of the specimens with small blisters, the pre-crack arrested at the blister-substrate interface. In those cases, subsequent testing resulted in a load-displacement response that showed a smooth transition to plastic bending with the load increasing to a maximum load value and then continuously decreasing. In such cases, the onset of crack growth was detected by an acceleration of load loss and confirmed by potential drop data. As shown in Fig. 2a, crack growth for specimens with small blisters proceeded into an *in-plane* hydride microstructure. Thus, the resulting crack growth initiation toughness $K_Q$ is that for through-thickness crack growth initiation into an in-plane hydride microstructure.

For specimens with deep blisters such as that illustrated during interrupted testing in Fig. 2b, the pre-cracking process in the bend testing at room temperature created a crack that propagated not only through the blister *but also* through the adjoining sunburst hydride field. Thus, prior the first small load drop in Fig. 3a, the crack has already propagated through the blister (≅ 215 μm) *and* through the sunburst hydrides (an additional ≈ 90 μm). Thus, in these cases, the initial pre-crack length at crack growth initiation (at the load drop at 150N) was the sum of the blister depth (215 μm) plus the depth (~90 μm) of sunburst hydride in the plane of the crack. After the load drop (Fig. 3b) the crack has propagated ≈ 40 μm into the mixed hydride field. Importantly, this crack growth sequence implies that the $K_Q$ -value at the 150N load drop corresponds to crack growth initiation into a mixed hydride microstructure. Further loading (Fig. 3c) results in large-scale yielding (specimen is plastically bent) and is characterized by crack arrest and significant crack-tip deflection. Crack growth into the in-plane hydride field is difficult, and a small degree of crack growth (≈ 25 μm in Fig. 3d) occurs only after significant far-field deformation of the specimen with crack-tip branching. The crack branching process is a result of large primary voids that form normal to the crack plane and along the broad faces of elongated hydrides ahead of the crack tip; see Fig. 3d.
Taken as a whole, the above behavior clearly indicates that at room temperature the through-thickness crack growth resistance is sensitive to the hydride microstructure. Specifically, the pre-crack growth through both the hydride blister *and* the sunburst hydrides suggests the ease of crack growth when the crack plane and crack growth direction coincides with the orientation of the hydride platelets, providing a continuity of crack path. These results also indicate that through-thickness crack growth initiation through microstructure containing a mixture of in-plane and out-of-plane hydrides is significantly easier than that for crack growth through large in-plane hydrides where crack branching and

deflection occurs. Thus, as discussed by Bertolino et al.[9, 20], fracture toughness is expected to be quite sensitive to hydride platelet orientation at room temperature.

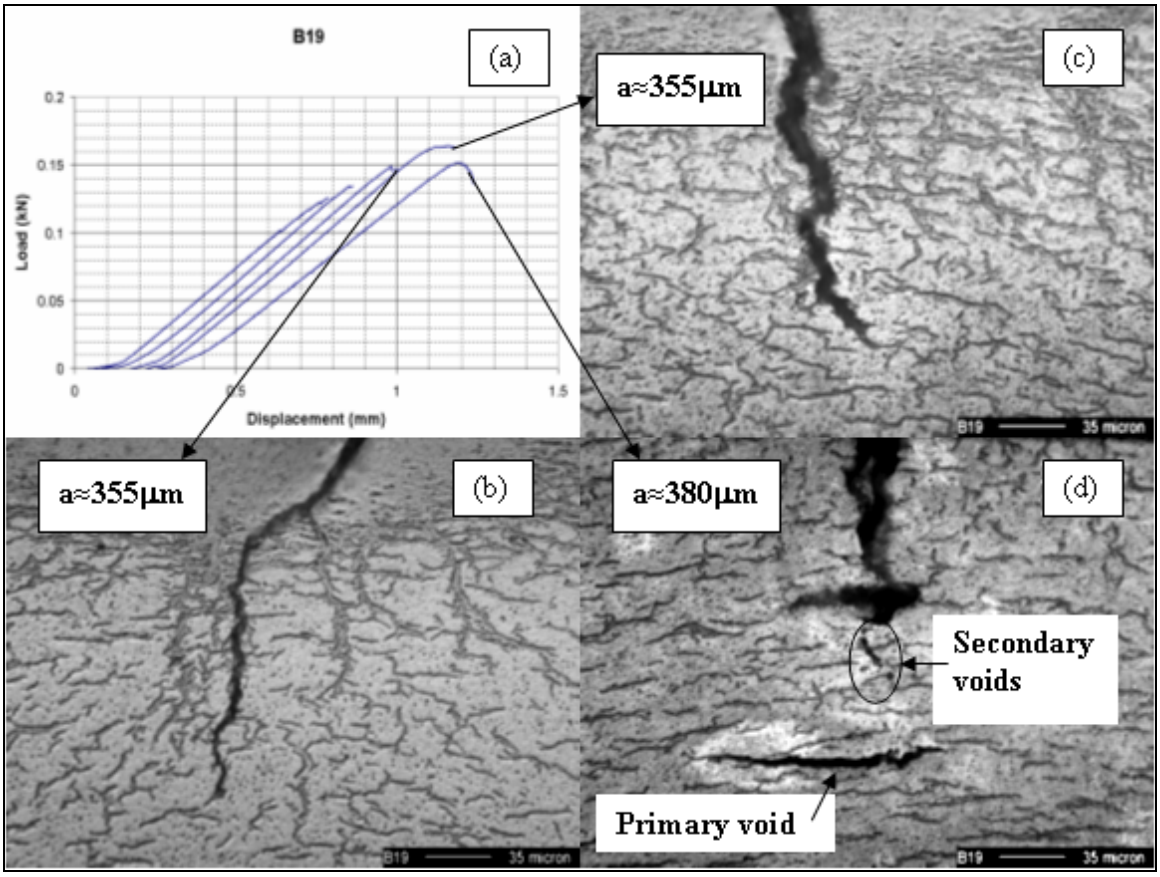


Fig. 3. The evolution of the crack profile with increased bending during the interrupted testing of a specimen with ≈215 μm blister. The test was performed at room temperature and onset of crack growth into mixed hydride field occurs at load drop at 150N

TABLE II

Fracture toughness values for through-thickness crack growth initiation in individual tests as a function of the hydride microstructure.

| **Temperature** | **Fracture Toughness** $K_Q$ | **Hydride Microstructure** |
|---|---|---|
| 25°C | 23, 27, and 28 MPa√m | Random/mixed hydrides with platelet orientations both in-plane and out-of-plane of the sheet. |
| 25°C | 66 and 80 MPa√m | Predominantly in-plane hydrides with significant presence of large particles that cause crack-tip branching. |

As shown in Table 2, the fracture toughness behavior is qualitatively consistent with the crack growth observations described above. Crack growth at room temperature through the field of mixed-orientation hydrides is characterized by a comparatively low fracture toughness, $K_Q \approx 25$ MPa√m. The lower fracture resistance is likely a reflection of the presence of significant amounts of radial hydrides in this mixed hydride field. We would expect that a low $K_Q$ -value in this case is promoted by cleavage or matrix-particle decohesion (which seems to be the case based on our initial fractography) along the faces of the hydride platelets aligned with the crack growth direction.

In contrast to the above behavior, $K_Q$ is much higher, ($K_Q \cong 75$ MPa√m), when the hydrides are oriented predominantly in the plane of the sheet and (importantly) normal to both the crack plane and the crack growth direction. In this case, despite the presence of elongated hydride particles that initiate large primary voids, their

presence also causes crack-tip deflection and crack branching (see Fig. 3d). The net effect is a $K_Q$ -value (75 MPa√m) that is close to $K_Q \cong 85$ MPa√m for *unhydrided* CWSR Zircaloy-4 cladding tube as determined by Bertsch and Hoffelner for axial crack growth.[21]. Thus, these results suggest that in-plane hydrides have only a minor net effect on through-thickness crack growth, at least at concentrations in the range of the present study.

Consistent with the crack growth behavior as viewed from specimen cross sections (Fig. 3), the fracture surfaces of specimens with large hydride blisters show distinct changes in appearance as the crack propagates. For example, Fig 4a shows that the fracture surface immediately beneath a comparatively large blister is relatively flat and characterized by shallow dimples and tear ridges. Such a fracture surface is consistent with a low energy fracture process as the crack propagates through both sunburst hydrides and a mixed hydride particle field containing a significant density of out-of-plane hydrides that create cleavage or void facets co-planar with the growing crack. The result is a comparatively low fracture toughness, $K_Q \approx 20$'s MPa√m.

At depths sufficiently beneath the hydride blister such that the crack propagates into the region of *in-plane* hydrides, large primary voids elongated in an orientation normal to the crack plane *and* growth direction are readily evident on the fracture surface formed at room temperature; see Fig. 4b. These large voids (>100μm in length) have an average spacing of ~60-80μm and correspond to the larger hydrides seen in metallographic observations of the Zircaloy-4 matrix (Fig. 2b). As discussed previously, the presence of large elongated in-plane hydrides cause crack deflection/branching, thus increasing the crack growth resistance ($K_Q \approx$70's MPa√m) relative to that observed in the mixed hydride region ($K_Q \approx$ 20's MPa√m). Although not reported here, a positive tearing modulus results as the crack grows into the in-plane hydride region.

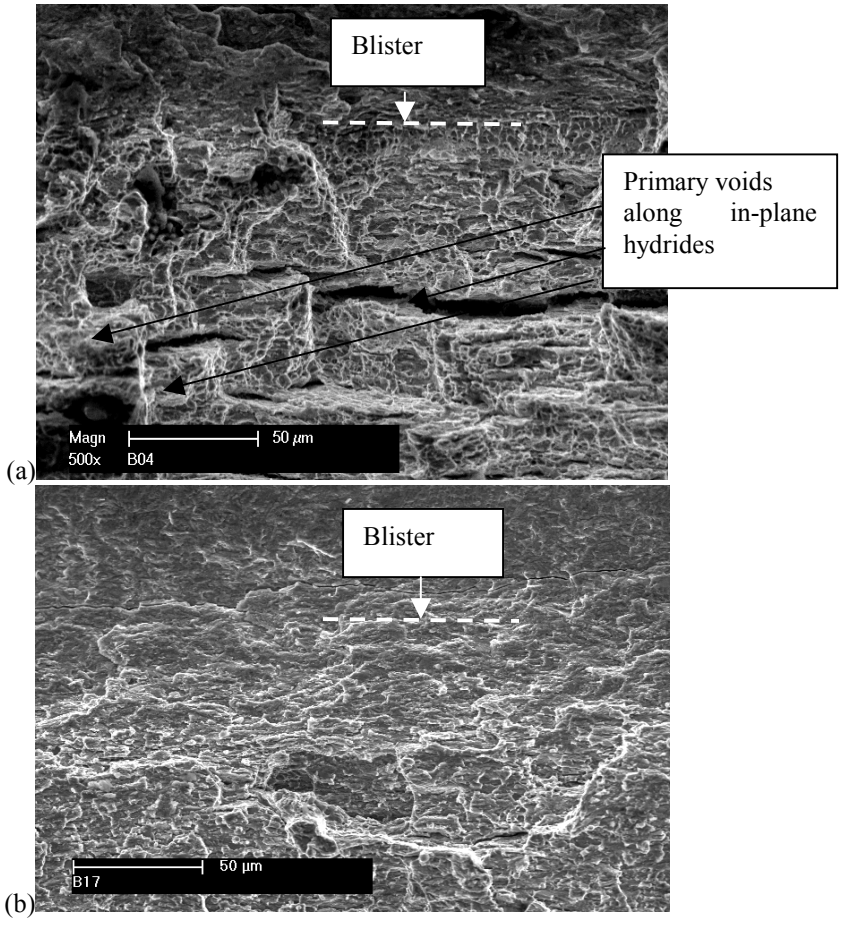


Fig. 4. Secondary electron SEM images of the fracture surfaces showing the region directly below the blister for (a) ~100μm blister specimen fractured at 25°C (b) and for a ~200μm blister specimen fractured at 25°C.

*III.C. Implications to Fracture strains*

In view of the magnitude of the fracture toughness values and their sensitivity to hydride orientation, we present here some examples of the fracture strain behavior predicted by the $K_Q$ -values in Table 2. Based on an elastic-plastic fracture mechanics analysis used by Pierron et al for predicting plastic strain at crack growth initiation in hydrided Zircaloy-4 cladding tube [22], the plastic strain at the onset of crack growth is given by:

$$\varepsilon_n^p = \alpha \frac{\sigma_0}{E}\left[\frac{1}{\alpha}\left(\frac{K_c^2}{K_e^2}-1\right)\right]^{\frac{n'}{n'-1}} \quad (5)$$

where $\sigma_0$ the yield strength, E the Young's modulus, $K_c$ the fracture toughness, n' is given by the Ramberg-Osgood relationship (and is the inverse of the strain-hardening exponent n):

$$\frac{\varepsilon}{\varepsilon_0} = \frac{\sigma}{\sigma_0} + \alpha\left(\frac{\sigma}{\sigma_0}\right)^{n'} \quad (6)$$

and $\alpha = \frac{\sigma_0^{n'-1}E}{k^{n'}}$ where k is the strength coefficient from the Ramberg-Osgood equation.

The elastic stress intensity factor corrected with the plastic zone adjustment is given by:

$$K_e = F\sigma\sqrt{\pi a_e} \quad (7)$$

where $a_e = a + r_{0\varepsilon} = a + \frac{1}{6\pi}\left(\frac{K_e}{\sigma_0}\right)^2$ (assuming plane strain) and

$\sigma = k\frac{\left[\varepsilon_n^p\sqrt{\frac{2(2+R)(1+R)}{3(1+2R)}}\right]^n}{\sqrt{\frac{(1+2R)}{(1+R)^2}}}$ where R is the plastic anisotropy parameter, and F the crack geometry correction factor is the standard relationship of either a semi-infinite crack or a semi-elliptical crack in tension in a panel of finite width W.

Based on the $K_Q$ -values in Table 2 and Eq's. 6 and 7, the predicted fracture strains are shown on Fig. 5 as a function of normalized crack depth. In addition, the predicted fracture strains are compared to experimental data [4, 6, 22] from Zircaloy-4 cladding tube with hydride rims, Fig 5a, and Zircaloy-4 sheet with hydride blisters, Fig 5b. In these experimental data [4, 6, 22], the hydride microstructures beneath the hydride rim or the hydride blister were predominantly circumferential hydrides in cladding tubes or in-plane hydrides in sheet specimens, with little or no radial-type hydrides. For very small flaw depths, fracture is not limited by crack growth, and thus the corresponding values of fracture strains of uncracked specimens subject to plane-strain tension in the hoop direction of the cladding are also included in Fig. 5.

The results in Fig. 5 show the strong sensitivity of fracture strain to both crack depth and $K_Q$-value. Specifically, Fig. 5 graphically illustrates that very small fracture strains are expected when even a small crack grows into a microstructure consisting of mixed hydrides where a significant fraction are co-planar with the crack and a small $K_Q$-value results (≈ 25 MPa√m). These results imply a marked sensitivity to crack-growth failure in cases where even a small crack might exist in the presence of radial hydrides.

In contrast, as in all of the experimental studies cited in Fig. 5, when through-thickness crack growth occurs into a hydride microstructure consisting predominantly of circumferential hydrides (in the case of cladding tubes) or in-plane hydrides (in the sheet specimens), significant plastic fracture strains can be expected as a consequence of the much higher fracture toughness (≈ 75 MPa√m). In fact, for very small flaw depths, the fracture strains predicted on the basis of crack growth exceed those of uncracked specimens, and failure is then not limited by crack growth. Finally, we take the good agreement in Fig. 5 between the experimentally determined fracture strains and the predicted values as a validation of both the measured $K_Q$ -values and the fracture mechanics analysis presented above.

(a)

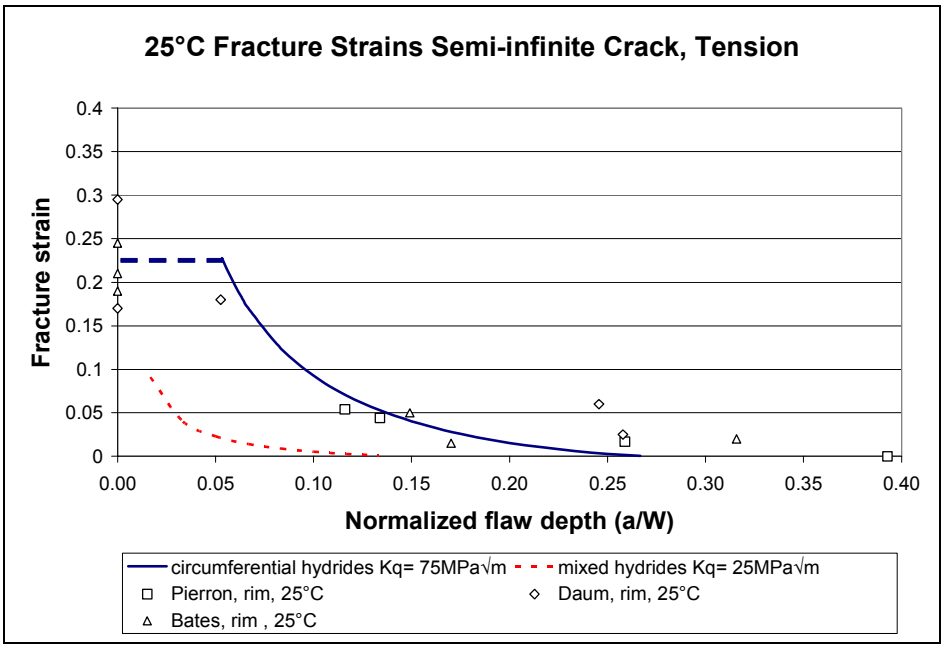


(b)

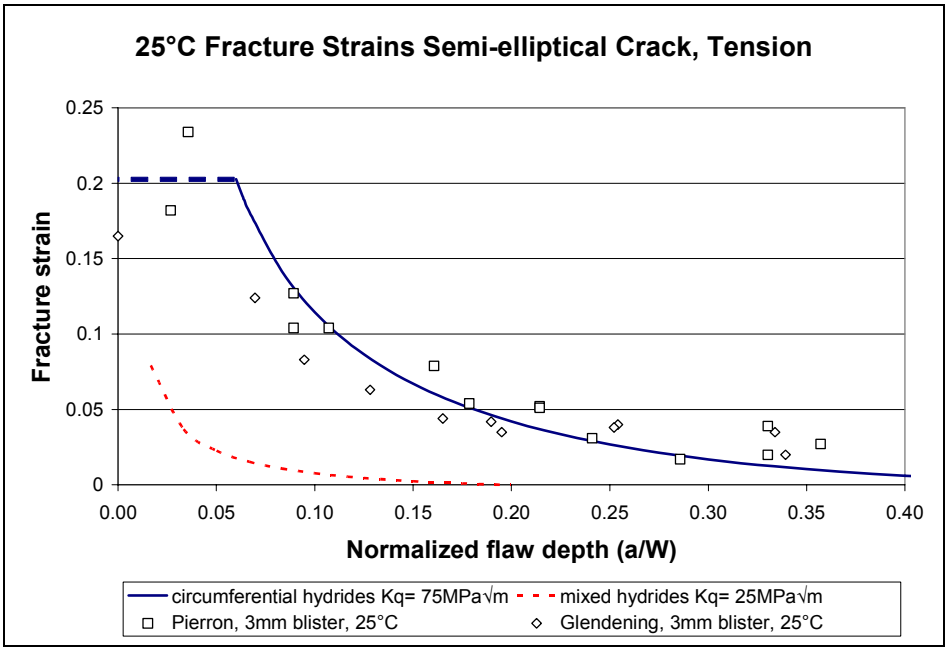


Fig. 5. Predicted fracture strains (solid lines) as a function of crack depth as compared to experimental data based on the plane-strain fracture of (a) ring-stretch hydrided Zircaloy-4 specimens containing a rim of dense hydrides that form a crack of rim depth (Experimental results are from Pierron et al [22] and Daum [6]) and (b) hydrided Zircaloy-4 sheet specimens containing blisters and fractured in either plane-strain tension (Pierron et al [22]) or equal-biaxial tension (Glendening et al [4]) The decrease in predicted fracture strains for $K_Q$ = 25 MPa√m is also included; see light dotted lines.

## IV. CONCLUSIONS

1. The fracture toughness of hydrided CWSR Zircaloy-4 sheet has been determined at room temperature under *through-thickness* crack growth conditions using a

novel procedure that on a narrow strip of brittle hydride blister to form a pre-crack upon initial loading. Crack growth initiation conditions occur under a plane-strain condition along the crack front and can be determined using elastic-plastic fracture mechanics analysis.

2. The fracture toughness is sensitive to the microstructure of the hydride particles beneath the solid hydride blister. For through-thickness crack growth within a mixed microstructure of in-plane and out-of-plane hydrides wherein a significant fraction of the hydride platelets are aligned parallel to the crack plane and crack growth direction, $K_Q \approx 25$ MPa$\sqrt{m}$. In contrast, preliminary results indicate that $K_Q$ is much higher, $K_Q \approx 75$ MPa$\sqrt{m}$, when the crack grows through a zone of in-plane hydride platelets oriented predominantly within the plane of the sheet (akin to circumferential hydrides in cladding tubes). In this latter case, crack deflection and crack branching occur as a result of the interaction between the crack and hydride platelets that are oriented normal to both the crack plane and crack growth direction.
3. Based on the experimentally determined fracture toughness values in this study, a fracture mechanics based analysis has been utilized to predict fracture strains as a function of normalized crack depth. The predicted results show good agreement with previous experimental studies of the fracture behavior of Zircaloy-4 in the form of both cladding tube containing hydride rims and sheet specimens with hydride blisters that are subject to either plane-strain or equal-biaxial loading. The predicted results also indicate a strong influence of hydride platelet orientation on fracture strains when a crack is present.

## ACKNOWLEDGMENTS

The authors gratefully acknowledge the financial support and encouragement from Ralph Meyer and Harold Scott at the Nuclear Regulatory Commission. Surface preparation prior to hydrogen charging was performed at the Penn State Nanofabrication facility. The authors also acknowledge helpful discussions with Christophe Poussard and Claude Sainte-Catherine of the CEA, as well as Jean Desquines at IRSN.

## REFERENCES

1. J. B. Bai, C. Prioul, and D. Francois, "Hydride Embrittlement in Zircaloy-4 Plate: Part I. Influence of Microstructure on the Hydride Embrittlement in Zircaloy-4 at 20 C and 350 C.," *Metallurgical and Materials Transactions A*, **25A**,*6*, p. 1185 (1994).
2. R. O. Meyer, R. K. McCardell, H. M. Chung, D. J. Diamond, and H. H. Scott, "A Regulatory Assessment of Test data for Reactivity Initiated Accidents," *Nuclear Safety*, **37**,*4*, p. 872 (1996).
3. A. M. Garde, G. P. Smith, and R. C. Pirek, "Effects of Hydride Precipitate Localization and Neutron Fluence on the Ductility of Irradiated Zircaloy-4," *Proc. of the 11th International Symposium on Zr in the Nuclear Industry*, STP 1295, p.407, ASTM International, West Conshochocken, PA (1996).
4. A. Glendening, D. A. Koss, O. N. Pierron, A. T. Motta, and R. S. Daum, "Failure of Hydrided Zircaloy-4 Under Equal-Biaxial and Plane-Strain Tensile Deformation," *Proc. of the Fourteenth International Symposium on Zirconium in the Nuclear Industry, ASTM STP 1467*, p.833, ASTM International, West Conshochocken, PA (2005).
5. T. M. Link, D. A. Koss, and A. T. Motta, "Failure of Zircaloy Cladding under transverse plane-strain deformation," *Nuclear Engineering and Design*, **186**, p. 379 (1998).
6. R. S. Daum, S. Majumdar, H. C. Tsai, M. C. Billone, D.W.Bates, D. A. Koss, and A. T. Motta, "Embrittlement of Hydrided Zircaloy-4 under RIA-like conditions," *Proc. of the 13th ASTM International Symposium on Zr in the Nuclear Industry*, STP 1423, p.702, ASTM (2001).
7. V. Grigoriev, B. Josefsson, and B. Rosborg, "Fracture Toughness of Zircaloy Cladding Tubes," *Proc. of the 11th ASTM International Symposium on Zr in the Nuclear Industry, ASTM STP 1295*, STP 1295, p.431, ASTM International, West Conshochocken, PA (1996).
8. P. H. Kreyns, W. F. Bourgeois, C. J. White, P. L. Charpentier, B. F. Kammenzind, and D. G. Franklin, "Embrittlement of reactor core materials," *Proc. of the Proceedings of the 1995 11th International Symposium on Zirconium in the Nuclear Industry, Sep 11-14 1995*, p.758, ASTM, Conshohocken, PA, USA (1996).
9. G. Bertolino, J. Perez Ipina, and G. Meyer, "Influence of the crack-tip hydride concentration on the fracture toughness of Zircaloy-4," *Journal of Nuclear Materials*, **348**,*1-2*, p. 205 (2006).
10. C. K. Chow and L. A. Simpson, "Analysis of the Unstable Fracture of a Reactor Pressure Tube Using Fracture Toughness Mapping," *in 'Case Histories Involving Fatigue and Fracture Mechanics'*, p.78, Charleston, SC, USA (1986).
11. J. J. Kearns and C. R. Woods, "Effect of texture, grain size, and cold work on the precipitation of oriented hydrides in Zircaloy tubing and plate," *Journal of Nuclear Materials*, **20**, p. 241 (1966).
12. P. Delobelle, P. Robinet, P. Bouffioux, P. Greyer, and I. LePichon, "A Unified Model to Describe the

Anisotropic Viscoplastic Zircaloy-4 Cladding Tubes," *Proc. of the 11th International Symposium on Zr in the Nuclear Industry*, STP 1295, p.373, ASTM, Philadelphia, PA (1996).

13. M. Nakatsuka, "Mechanical Properties of Neutron Irradiated Fuel Cladding Tube.," *Journal of Nuclear Science and Technology*, **28**,*4*, p. 356 (1991).
14. A. Saxena and C. L. Muhlstein, "Crack Length Measurement," *in ' Mechanical Testing and Evaluation'*, p.174, (2000).
15. T. L. Anderson, *Fracture Mechanics Fundamentals and Applications*, Taylor and Francis/CRC press, 2005.
16. Y. J. Kim, "Plastic eta factors based on load-CMOD records for SE(B) toughness testing specimens," *Key engineering materials*, **183-187**, p. 133 (2000).
17. Y. J. Kim, "Experimental J estimation equations for single-edge-cracked bars in four-point bend: homogeneous and bi-material specimens," *Engineering Fracture Mechanics*, **69**, p. 793. (2002).
18. M. T. Kirk and R. H. Dodds, "J and CTOD estimation equations for shallow cracks in single edge notch and bend specimens," *Journal of testing and evaluation,*, **21**, p. 228 (1993).
19. O. N. Pierron, D. A. Koss, A. T. Motta, and K. S. Chan, "The Influence of Hydride Blisters on Fracture of Zircaloy 4," *Journal of Nuclear Materials*, **322**, p. 21 (2003).
20. G. Bertolino, G. Meyer, and J. Perez Ipina, "Effects of hydrogen content and temperature on fracture toughness of Zircaloy-4," *Journal of Nuclear Materials*, **320**,*3*, p. 272 (2003).
21. J. Bertsch and W. Hoffelner, "Crack resistance curves determination of tube cladding material," *Journal of Nuclear Materials*, **352**,*1-3*, p. 116 (2006).
22. O. N. Pierron, D. A. Koss, A. T. Motta, and K. S. Chan, "The influence of hydride blisters on the fracture of Zircaloy-4," *Journal of Nuclear Materials*, **322**, p. 21 (2003).